⌘ *Author's Choice*

Hyaluronan Mixed Esters of Butyric and Retinoic Acid Affording Myocardial Survival and Repair without Stem Cell Transplantation[*][S]

Vincenzo Lionetti[‡§1], **Silvia Cantoni**[¶‖1], **Claudia Cavallini**[¶], **Francesca Bianchi**[¶], **Sabrina Valente**[**], **Irene Frascari**[¶], **Elena Olivi**[¶], **Giovanni D. Aquaro**[§], **Francesca Bonavita**[¶], **Ignazio Scarlata**[¶], **Margherita Maioli**[‡‡], **Valentina Vaccari**[¶], **Riccardo Tassinari**[¶], **Antonietta Bartoli**[§§], **Fabio A. Recchia**[‡¶¶], **Gianandrea Pasquinelli**[**], and **Carlo Ventura**[¶‖2]

*From the ‡Sector of Medicine, Scuola Superiore S. Anna, I-56124 Pisa, Italy, the ¶Laboratory of Molecular Biology and Stem Cell Engineering, Cardiovascular Department-National Institute of Biostructures and Biosystems, S. Orsola-Malpighi Hospital, University of Bologna, I-40138 Bologna, Italy, the ‖Bioscience Institute, RSM-47891 Falciano, Republic of San Marino, the §Institute of Clinical Physiology, Consiglio Nazionale delle Ricerche Fondazione G. Monasterio, I-56124 Pisa, Italy, the ‡‡Department of Biomedical Sciences, University of Sassari, I-07100 Sassari, Italy, the §§Department of Physics, University of Pisa, I-56124 Pisa, Italy, the ¶¶Department of Physiology, New York Medical College, Valhalla, New York 10595, and the **Department of Hematology, Oncology, and Clinical Pathology, University of Bologna, I-40138 Bologna, Italy*

Possible cardiac repair by adult stem cell transplantation is currently hampered by poor cell viability and delivery efficiency, uncertain differentiating fate *in vivo*, the needs of *ex vivo* cell expansion, and consequent delay in transplantation after the onset of heart attack. By the aid of magnetic resonance imaging, positron emission tomography, and immunohistochemistry, we show that injection of a hyaluronan mixed ester of butyric and retinoic acid (HBR) into infarcted rat hearts afforded substantial cardiovascular repair and recovery of myocardial performance. HBR restored cardiac [18F]fluorodeoxyglucose uptake and increased capillary density and led to the recruitment of endogenous Stro-1-positive stem cells. A terminal deoxynucleotidyl-transferase-mediated dUTP nick end labeling assay demonstrated that HBR-treated hearts exhibited a decrease in the number of apoptotic cardiomyocytes. In isolated rat cardiomyocytes and Stro-1 stem cells, HBR enhanced the transcription of vascular endothelial growth factor, hepatocyte growth factor, *kdr*, *akt*, and *pim-1*. HBR also increased the secretion of vascular endothelial growth factor and hepatocyte growth factor, suggesting that the mixed ester may have recruited both myocardial and Stro-1 cells also. An increase in capillarogenesis was induced *in vitro* with medium obtained from HBR-exposed cells. In the infarcted myocardium, HBR injection increased histone H4 acetylation significantly. Acetyl-H4 immunoreactivity increased in rat cardiomyocytes and Stro-1 cells exposed to HBR, compared with untreated cells. In conclusion, efficient cardiac regenerative therapy can be afforded by HBR without the need of stem cell transplantation or vector-mediated gene delivery.

Cardiomyocyte loss during myocardial infarction (MI)[3] is associated with dysfunction of underperfused myocardium, eventually progressing toward heart failure. Analysis of the rescuing potential associated with transplantation of human mesenchymal stem cells (hMSCs) in animal models of MI has recently led to the conclusion that paracrine actions exerted by adult stem cells through the release of soluble factors might be important mechanisms of tissue repair and functional improvement (1, 2). To this end, we have recently shown that hMSCs isolated from fetal membranes of human term placenta (FMhMSCs) secreted large amounts of angiogenic, mitogenic, antiapoptotic, and antifibrotic factors, as compared with hMSCs isolated from the human bone marrow, significantly contributing to improved cardiovascular function in infarcted rat hearts (3). It is noteworthy that *ex vivo* preconditioning of FMhMSCs with a mixed ester of hyaluronan with butyric and retinoic acid (HBR) acted transcriptionally to increase both the commitment to cardiovascular lineages and the secretion of trophic mediators, remarkably enhancing stem cell-mediated improvement *in vivo* (3).

Here, we directly injected HBR into the myocardium of infarcted rat hearts and provide evidence that the mixed ester afforded substantial recovery of myocardial performance without the need of stem cell transplantation. The HBR action was also associated with an increase in the number of Stro-1-posi-

[3] The abbreviations used are: MI, myocardial infarction; HBR, hyaluronan mixed ester of butyric and retinoic acid; VEGF, vascular endothelial growth factor; HGF, hepatocyte growth factor; hMSC, human mesenchymal stem cell; MRI, magnetic resonance imaging; PET, positron emission tomography; mPET, small animal positron emission tomography; [18F]FDG, [18F]fluorodeoxyglucose; RCm, rat neonatal cardiomyocyte(s); RAOECs, rat aortic endothelial cells; HUVEC, human umbilical vein endothelial cell(s); DS, degree of substitution; LV, left ventricular; vWF, von Willebrand factor; TBS, Tris-buffered saline; Ab, antibody; GAPDH, glyceraldehyde-3-phosphate dehydrogenase; HA, hemagglutinin; BU, butyric acid; RA, retinoic acid; PBS, phosphate-buffered saline; PDGF, platelet-derived growth factor.

tive cells within the injected myocardium. These responses probably involved the activation of a gene program of paracrine patterning for myocardial protection and angiogenesis and the enhanced survival of locally recruited stem cells.

EXPERIMENTAL PROCEDURES

Synthesis of HBR—The procedure for the synthesis and characterization of HBR, and the related chemical structure are reported in detail elsewhere (4). The primary hydroxyl group in position 6 of the *N*-acetyl-D-glucosamine residues in the polysaccharide backbone is the most reactive toward esterification. Briefly, we prepared a double salt of tetrabutylammonium with two functional groups of hyaluronan, specifically its carboxyl and 6-hydroxyl, in order to achieve good solubility in polar aprotic organic solvents and to increase the nucleophilicity of the oxygen atom at C-6. Retinoylation with retinoyl chloride, which is the rate-limiting step, was carried out before butyrylation by means of butyric anhydride and 4-(dimethylamino)pyridine as a hypernucleophilic acylation catalyst (4). The degree of substitution (DS) was considered as the number of the esterified OH groups for each repeating unit of hyaluronic acid (GlcNAc-GlcUA dimer). The weight-average molecular weight of HBR, referred to as the weight-average of sodium hyaluronate, was determined by high performance size exclusion chromatography (4).

Myocardial Infarction (MI)—Studies were performed on male Wistar rats ($n = 30$, 250–300 g in size). Animals were sedated (xylazine 14 mg/kg, intraperitoneally), anesthetized (Zoletil100, 40 mg/kg, intraperitoneally), and ventilated with a mixture of air and oxygen (1:1), and MI was induced as described previously (3). Briefly, a thoracotomy was performed in the left fourth intercostal space, and a permanent surgical ligation was placed around the left anterior descending coronary artery near its origin with a 6-0 silk suture, during electrocardiographic monitoring for ST changes and arrhythmias. The chest was closed in layers, and pneumothorax was reduced. Experimental protocols were approved by the Animal Care Committee of the Italian Ministry of Health, in accordance with Italian law (DL-116, January 27, 1992).

Healthy animals were randomly divided into three experimental groups: 1) MI treated with 100 μl of sterile phosphate-buffered saline (PBS) as vehicle (control group, MI + PBS, $n = 10$), 2) MI treated with 100 μl of HBR solution (0.2 mg of HBR per 100 g of rat weight) (treated group, MI + HBR, $n = 10$), and 3) sham-operated rats (SHAM, $n = 10$), in which left anterior descending coronary artery was not occluded. The sterile solutions were injected into the viable myocardium bordering the infarct zone and the infarcted site 45 min after the coronary ligation by a syringe with a needle of 24 gauge. The infarct zone was identified by the pale color of the myocardium. Small animal positron emission tomography (mPET) and 1.5-tesla magnetic resonance imaging (MRI) were performed 4 weeks after coronary ligation.

Functional Assessment—Regional left ventricular (LV) myocardial glucose uptake was measured by mPET to assess oxidative metabolism, whereas regional contractility and infarct size were quantified by conventional MRI. For both types of imaging, we used three cross-sectional planes (*i.e.* basal, middle, and

apical) and six circumferential regions (*i.e.* anterior, anterior-lateral, inferolateral, inferior, inferoseptal, and anterior-septal). LV regions were selected as described previously (5). Briefly, the infarcted area comprised segments with more than 25% of their area occupied by scar tissue, and the border zone comprised segments containing less than 25% of scar tissue area and was immediately contiguous (either circumferentially or longitudinally) to the infarcted area. The remote segments that did not contain scar tissue were those located outside the border zone. To assess the relationship between *in vivo* measurements of myocardial contractility and metabolism, mPET was performed within 24–36 h after MRI.

MRI Measurements—MRI protocol was performed with a 1.5-tesla clinical whole body scanner (Signa CVI, GE Medical Systems) by using a phased array send-receive coil for a human knee (knee PA coil), as described previously (6). An electrocardiograph-triggered SSFP (FIESTA) pulse sequence was acquired to assess LV function (parameters: 200-mm field of view, 3-mm slice thickness, no gap, number of excitations 5, two views per segment, echo time/repetition time 1.6/3.2, flip angle 45°, matrix 192 × 192, and reconstruction matrix 256 × 256). In each rodent, a total of four LV short axis (to completely cover ventricular main axis in end diastole) and two LV long axis views (vertical and horizontal long axis) were acquired. For each view, 10 cine frames were acquired. For detection of non-viable myocardium, which appears hyperintense, and for assessment of LV infarct size, delayed enhancement images were obtained 3 min after bolus injection of Gadobutrol (Gadovist®; 0.02 mmol per 100 g of body weight) via the tail vein; images were acquired in the same short axis and long axis slices as used for cine MRI. An electrocardiograph-triggered fast gradient echo inversion recovery pulse sequence was utilized with the following parameters: TR 4.2 ms, TE minimum, flip angle 20°, matrix 192 × 192, NEX 5, field of view 20–20 mm, slice thickness 3 mm, no interslice gap, 1 R-R interval. The inversion time was fixed to 100 ms and eventually optimized to null signal from the normal myocardium when appropriate.

Image Processing—To assess the infarct size, the extent of delayed enhanced areas was measured using a semiautomatic software, previously validated by us (7). For this purpose, we used all short axis images and two additional long axis images for the analysis of the cardiac apex. In each image, the boundaries of contrast-enhanced areas were traced and manually corrected when needed. Contrast-enhanced regions, namely the infarcted regions, were expressed in grams as well as in percentage of the entire left ventricle. Left ventricle end diastolic and end systolic volumes, LV mass, and ejection fraction were measured from the cine images using previously validated software (Mass®, MEDIS).

The infarcted region was detected in cine images by comparison with the respective delayed enhancement image. Then regional end diastolic and end systolic wall thickness was measured in the core of the infarcted area, in the border regions, and in the remote myocardium. Regional contractility was assessed by employing the end systolic wall thickening in three short-axis segments (basal, middle, and apical) for correlations with matched PET slices. Absolute regional wall thickening was calculated in the same regions by the difference between end sys-

tolic and end diastolic wall thickness. Relative regional wall thickening was calculated with the formula, end systolic/end diastolic wall thickness × 100, and expressed as a percentage.

PET Measurements—Each sedated rat was placed on a scanner bed in prone position and received an intravenous injection of [^{18}F]fluorodeoxyglucose ([^{18}F]FDG; 45 MBq) via the tail vein in a 0.15-ml volume. The residual dose in the syringe was measured to verify the effective injected dose. The heart was centered on the field of view. PET was performed with a small animal positron emission tomograph (GE eXplore Vista DR, GE Healthcare) (8). The dynamic list mode acquisition was immediately started for a total time of 30 min. Once the scan was finished, animals were placed in a recovery box with a warm temperature until complete recovery. All images were reconstructed with iterative reconstruction on OSEM 2D (Siemens) and visualized frame by frame with dedicated software in three planes (axial, sagittal, and coronal), as described previously (9). To perform viability analysis in each experimental condition, dynamic scans were reformatted by adding all frames of the last 10 min of acquisition in order to obtain a static acquisition image. Semiquantitative analysis of regional LV [^{18}F]FDG uptake was performed with specific software adapted for animals (ECTB) (9, 10), using resting scores of 0–4 (0, normal; 1, equivocal; 2, moderately reduced; 3, severely reduced; 4, absent).

Tissue Immunohistochemistry—Hearts were arrested in diastole, and 3-mm-thick transverse slices were cut through the short axis of both ventricles at midseptal level. Macroscopic infarct size was assessed by nitro blue tetrazolium staining. Samples were fixed in 10% buffered formalin and embedded in paraffin, and 4-μm-thick sections were used for histological, immunohistochemical, and immunofluorescence analysis. For conventional histopathological analysis, sections were stained with hematoxylin and eosin. Picro-Mallory trichrome staining was used for determining the degree of fibrosis. Images were digitized through a video camera (JVC 3CCD video camera, KY-F55B) connected with a Leitz diaplan light microscope; original images were taken at ×10 and analyzed using Image-Pro Plus® 6 software (Media Cybernetics, Inc.).

Four-μm-thick dewaxed sections were used for immunohistochemical studies. Capillary density was assessed by a polyclonal antibody against von Willebrand factor (vWF). Stem cell recruitment (mesenchymal cells or mononuclear cells) into the infarcted myocardium was assessed using antibodies directed against Stro-1 and c-Kit antigens, respectively. Cycling cells were identified with an antibody against nuclear transcription factor Ki-67. The accumulation and the spatial distribution of acetyl-histones was investigated with an antibody directed against acetyl-histone H4. Perivascular cells were characterized using antibodies against NG2 and PDGF-Rβ, and expression of vascular endothelial growth factor (VEGF) was detected with an antibody recognizing all VEGF isoforms. Specimens were deparaffinated with xylene, rehydrated through decreasing concentrations of ethanol, rinsed in distilled water, and subjected to an antigen retrieval treatment. Antigens were unmasked with citrate buffer, pH 6.0, at 120 °C, 1 atm for 21 min. After cooling and washing, endogenous peroxidase activity was neutralized using a 3% H_2O_2 solution in metha-
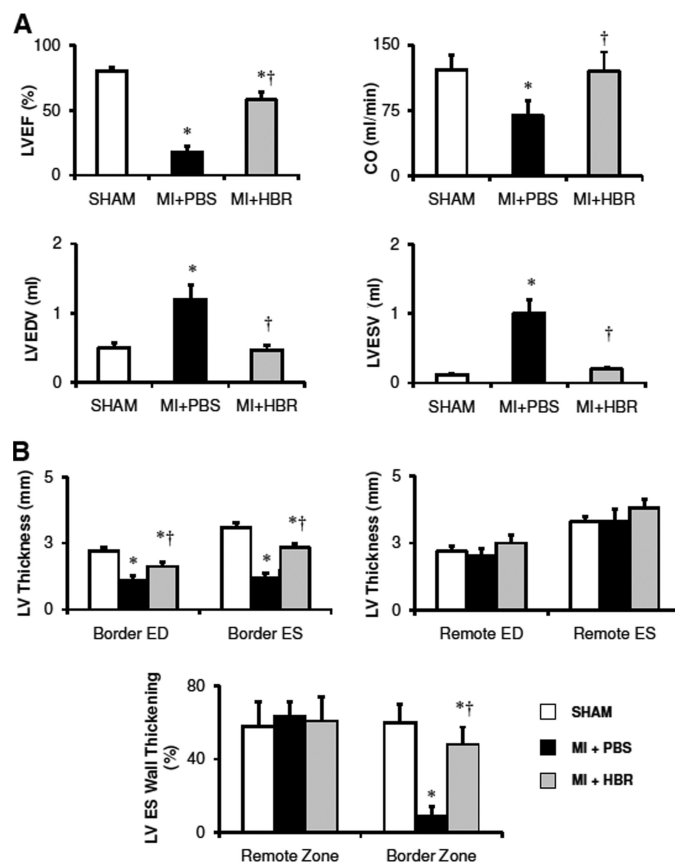

FIGURE 1. **MRI-derived measures of left ventricular function.** Global (*A*) and regional (*B*) LV function are shown. Values are means ± S.E.; $n = 11$ animals for each experimental condition. *LVEF*, LV ejection fraction; *CO*, cardiac output; *LVEDV*, LV end diastolic volume; *LVESV*, LV end systolic volume; *ED*, end diastolic; *ES*, end systolic. The HBR-treated group received 100 μl of HBR solution (0.2 mg of HBR/100 g of rat weight). *, $p < 0.05$ *versus* SHAM; †, $p < 0.05$ *versus* MI + PBS (one-way analysis of variance with subsequent Bonferroni test).

nol absolute for 10 min at room temperature in the dark; sections were then processed for immunohistochemistry with a non-biotin-amplified method (NovoLink^{TM} Polymer Detection System, Novocastra Laboratories Ltd.). After washing with 1× TBS, the slides were incubated with Novocastra^{TM} protein block for 5 min in a wet chamber to reduce the nonspecific binding of primary antibody and polymer reagent and rinsed twice with 1× TBS. Tissue sections were subsequently stained using monoclonal antibodies against Stro-1 (1:100; R & D Systems, Inc.), Ki-67 (1:230, clone MM1; Novocastra), NG2 (1:100; R&D Systems, Inc.), PDGF-Rβ (1:100; R&D Systems, Inc.), and polyclonal antibodies against acetyl-histone H4 (1:150, Lys8; Upstate Biotechnology), c-Kit (1:200, DakoCytomation), VEGF (1:50, JH121 clone; Abcam), vWF (1:2000; DakoCytomation) in 1% bovine serum albumin in PBS overnight at 4 °C. After washing, slides were incubated for 30 min at room temperature with Novocastra^{TM} post-primary block to enhance penetration of the next polymer reagent, rinsed in 1× TBS, and incubated with NovoLink^{TM} Polymer for 30 min at room temperature. After washing, the sections were exposed to the substrate/chromogen 3,3′-diaminobenzidine prepared from Novocastra^{TM} 3,3′-diaminobenzidine chromogen and
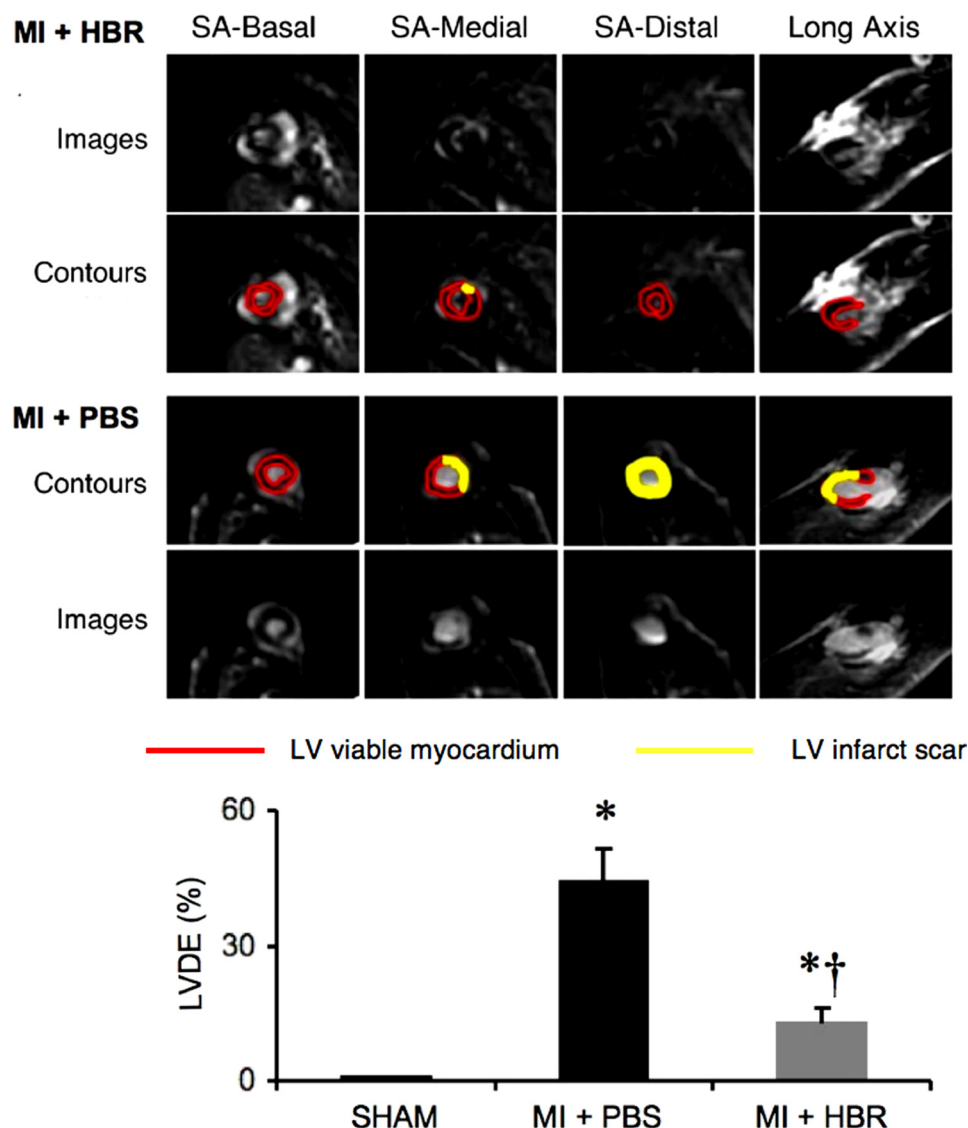
FIGURE 2. **MRI delayed contrast enhancement of myocardial scar.** *Top*, representative LV short and long axis gadolinium-delayed contrast-enhanced MRI images for each experimental condition. *Bottom*, regional LV delayed enhancement in infarcted LV treated with 100 μl of HBR solution (0.2 mg of HBR/100 g of rat weight) or PBS. Values are means $\pm$ S.E.; $n = 11$ animals for each experimental condition. *SA*, short axis; *LVDE*, LV delayed contrast enhancement. *, $p < 0.05$ *versus* SHAM; †, $p < 0.05$ *versus* MI + PBS (one-way analysis of variance with subsequent Bonferroni test).

formed as described above. Then sections were incubated for 30 min at room temperature in a wet chamber with blocking solution containing sheep serum (1:10) in 1% bovine serum albumin to reduce nonspecific staining. Tissue sections were labeled with the Stro-1 monoclonal antibody (1:100; R&D Systems) at 37 °C for 45 min in a wet chamber. After rinses, slides were incubated with a Cy3-conjugated sheep anti-mouse secondary antibody (1:1000; Sigma), in 1% bovine serum albumin in PBS for 45 min at 37 °C; sections were then treated with goat serum (1:10) or 2% rabbit serum in 1% bovine serum albumin in PBS for 30 min at room temperature and stained with anti-CD45 (1:100; Santa Cruz Biotechnology, Inc.) or anti α-sarcomeric actin monoclonal antibody (1:500; Sigma) or anti-c-Kit (1:200; DakoCytomation) or anti-vWF polyclonal antibodies (1:2000; DakoCytomation); all immunostainings were performed for 45 min at 37 °C in the dark. The slides were then incubated in polyclonal goat anti-rabbit fluorescein isothiocyanate-conjugated (fluorescein isothiocyanate, 1:500; Sigma) or rabbit anti-mouse fluorescein isothiocyanate-conjugated (fluorescein isothiocyanate, 1:250; DakoCytomation) antibodies for 45 min at 37 °C in the dark. Finally, after several rinses, the samples were coverslipped with ProLong antifade reagent with 4′,6-diamidino-2-phenylindole (Molecular Probes). For negative control, sections were processed omitting the primary antibody.

Gene Expression—Total RNA was extracted using TRIzol reagent (Invitrogen), and 1 μg was reverse-transcribed into cDNA in a 21-μl reaction volume with SuperScript™ III reverse transcriptase. To assess gene expression, 2 μl of cDNA were used for Real Time PCR performed with a Lightcycler system (Roche Applied Science) and with the SYBR Green I FastStart kit (Lightcycler® FastStart DNA MasterPLUS SYBR Green I) following the manufacturer's instructions. Primer sequence is reported in the supplemental material.

Data were normalized using GAPDH as an index of cDNA content after reverse transcription. Amplification included initial denaturation at 95 °C for 10 min, 50 cycles of denaturation at 95 °C for 10 s, annealing at 59–63 °C for 6–10 s, and extension at 72 °C for 10 s, performed at a temperature transition rate of 20 °C/s. Fluorescence was measured at the end of each exten-
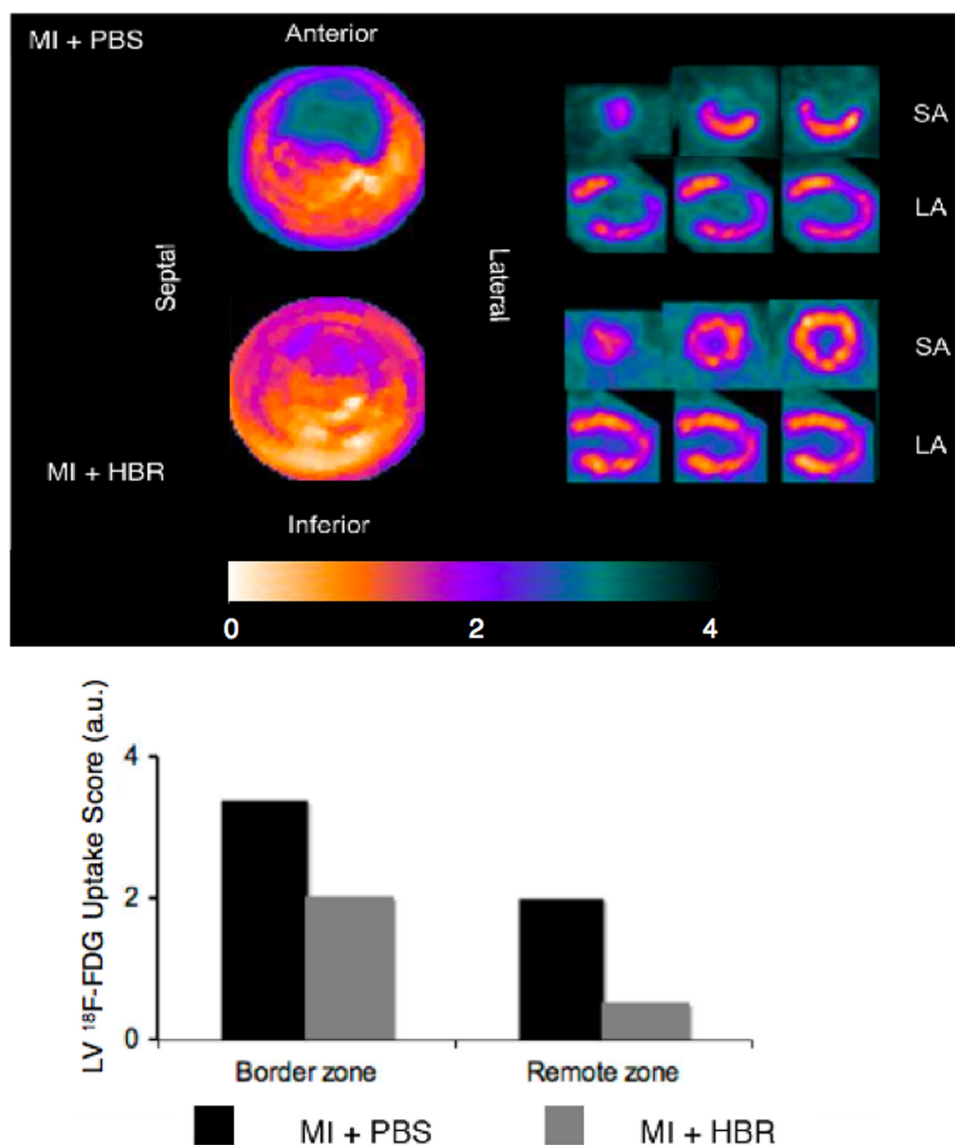
NovoLink™ 3,3′-diaminobenzidine substrate buffer, rinsed in distilled water, and counterstained with Gill's hematoxylin. Then samples were dehydrated, coverslipped, and viewed by light microscopy using the Image-Pro Plus® program. Negative control was obtained by omitting the primary Abs. Assessment of apoptotic programmed cell death by terminal deoxynucleotidyltransferase-mediated dUTP nick end labeling assay is described in the supplemental material.

Immunofluorescence—To investigate the co-expression of different antigens in the same cell, a double immunofluorescence procedure was used. We aimed to demonstrate whether Stro-1-positive cells co-expressed c-Kit, vWF, CD45, and α-sarcomeric actin, respectively. Four-μm-thick dewaxed sections were rehydrated with decreasing concentrations of ethanol and rinsed in distilled water. Antigen retrieval was per-

FIGURE 3. **Myocardial glucose uptake measured by [¹⁸F]FDG.** *Top*, representative LV polar map, short and long axis mPET images for each experimental condition; *Bottom*, mean score values of myocardial [¹⁸F]FDG of infarcted LV treated with 100 μl of HBR solution (0.2 mg of HBR/100 g of rat weight) or PBS. $n = 11$ animals for each experimental condition. *SA*, short axis; *LA*, long axis. *a.u.*, arbitrary units.

RNA (about 5×10^6 cpm) were then subjected to a solution hybridization RNase protection assay and were hybridized for 12 h at 55 °C in the presence of unlabeled antisense VEGF and *pim-1* mRNA. To generate these cRNA probes, cDNA fragments of rat VEGF (597 bp), *pim-1* (609 bp), or GAPDH (574 bp) genes were inserted into a pCRII-TOPO vector. Transcription of plasmids linearized with BamHI generated antisense strands of Pim-1 and GAPDH mRNA, whereas transcription of plasmids linearized with XbaI produced an antisense strand of VEGF mRNA. Samples were then incubated with a combination of RNase A and T1 and exposed to proteinase K. The protected fragments were recovered after phenol chloroform extraction and electrophoretically separated in a polyacrylamide non-denaturing gel. Autoradiographic exposure was for 48 h.

In Vitro Vasculogenesis Assay—Analysis of capillary-like tube formation was performed using extracellular matrix gel (Sigma). Fifty μl of gel matrix solution, diluted 1:2 with Dulbecco's modified Eagle's medium, was applied to each well on a 96-well plate and incubated for 1 h at 37 °C. Human umbilical vein endothelial cells (HUVECs) (Lonza) and rat aortic endothelial cells (RAOECs) (Cell Applications, Inc.) were cultured in endothelial growth medium (EGM-2 from Lonza and RAOEC growth medium from Cell Applications, Inc., respectively) until confluence. They were then trypsinized and seeded on the preprepared polymerized gel. For each well, 1×10^4 cells were suspended in 50 μl of conditioned medium obtained from rat neonatal cardiomyocytes (RCm) (Cell Applications, Inc.) or rat Stro-1-positive cells (ScienCell) cultured for 24 h in the absence or presence of HBR (2 mg/ml) and incubated at 37 °C. Capillary-like structures were observed after 2 h and at regular intervals during the following 24 h and photographed using an inverted optical microscope equipped with a digital sight camera (Nikon).

Enzyme-linked Immunosorbent Assay—VEGF and hepatocyte growth factor (HGF) were determined in supernatants harvested from RCm and Stro-1-positive cells cultured in the presence or absence of HBR (2 mg/ml) at different times (12 h, 24 h, 3 days, and 6 days) by using commercially available kits (rat VEGF enzyme-linked immunosorbent assay kit (R&D Systems) and rat HGF enzyme-linked immunosorbent

sion step. Specificity of the product was determined by a melting curve analysis, conducted after completion of the cycling process with the aid of a temperature ramp (from 55 to 95 °C at 0.1 °C/s) and continuous fluorescence monitoring. Samples were run in duplicate, and the average threshold cycle (*Ct*) value was used for calculations. Relative quantification of mRNA expression was calculated with the comparative *Ct* method using the "delta-delta method" for comparing relative expression results between treatments in real time PCR (11).

Nuclear Run-off Transcription Assay—Isolation of nuclei and assessment of nuclear purity were performed as detailed elsewhere (3). Only freshly isolated nuclei were used in each experiment. Nuclear run-off experiments were carried out as described previously (3). Nuclear RNA was isolated by using guanidine thiocyanate and acid phenol extraction, followed by purification on RNAMATRIX™. Equal counts of ³²P-labeled
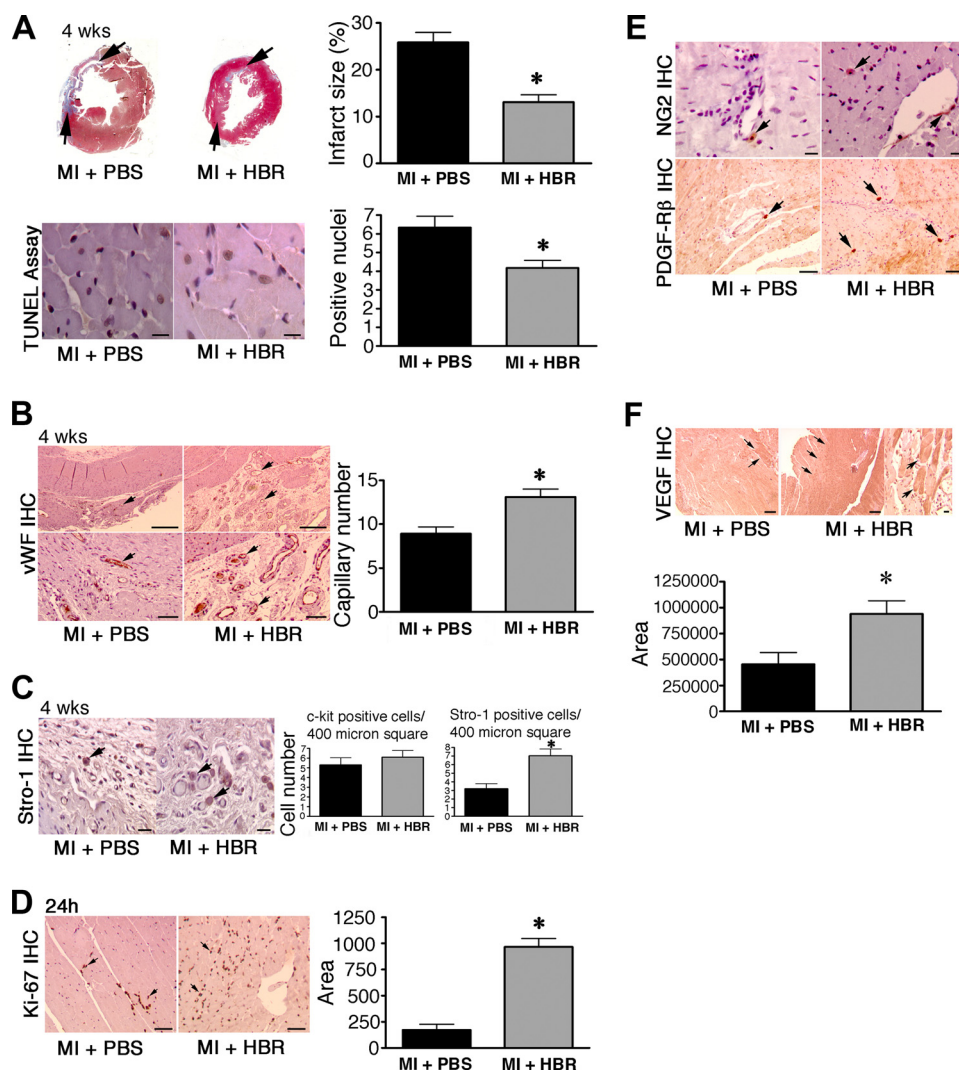
FIGURE 4. **HBR increased the number of capillary vessels, Stro-1-positive cells, and perivascular elements.** *A–C*, 4 weeks following myocardial infarction. Transversally cut left ventricular myocardium from HBR-treated (100 μl of HBR solution) hearts showed a reduced scar, compared with PBS-treated animals (*A, upper images, arrows* demarcate the infarcted area). Picro-Mallory stains in *blue* the area of scar and in *red* the myocardium parenchyma. In the border zone of HBR-treated hearts, scar reduction was associated with fewer apoptotic cardiomyocytes (*A, lower images; scale bars*, 20 μm) and increased number of capillary vessels (*B*). vWF expression highlights endothelial cells (*arrows*) lining the capillary inner wall (*B, scale bars*, 300 μm (*upper images*) and 50 μm (*lower images*). *C*, in HBR-treated samples, Stro-1 positive cells (*arrows*) increased in number and were closely associated with the outer capillary wall, whereas c-Kit-positive cells did not vary significantly, compared with untreated animals. *Scale bars*, 20 μm. *D–F*, 24 h following myocardial infarction. *D*, the number of Ki-67-positive cells significantly increased in the HBR-treated animals (*arrows*); *scale bars*, 50 μm. *E*, cells expressing NG2 and PDGF-Rβ (*arrows*); *scale bars*, 30 μm (*upper images*) and 100 μm (*lower images*). *F*, VEGF expression (*arrows*). *Scale bars*, 100 μm (*left* and *middle images*) and 50 μm (*right image*). ***, significantly different from PBS-treated hearts, $p < 0.05$ (statistical test: two-tailed, unpaired Student's t test). *IHC*, immunohistochemistry. Full-size images of each individual *panel* are presented in supplemental Fig. 1.

Western blotting detection reagents (GE Healthcare) according to the manufacturer's instructions.

Statistical Analysis—Statistical analysis was performed using GraphPad Prism, version 4. Data were evaluated by using a two-tailed, unpaired Student's t test and analysis of variance as appropriate, with the Bonferroni post hoc test, assuming a p value less than 0.05 as the limit of significance.

RESULTS

The glycoconjugate HBR is an ester between the hydroxyl groups of hyaluronan (HA) and the carboxyl groups of both butyric acid (BU) and retinoic acid (RA). All of the synthesized HBR exhibited a DS with BU (DS_{BU}) ranging between 0.05 and 1.5, whereas the DS with RA (DS_{RA}) was between 0.002 and 0.1. The DS_{BU}/DS_{RA} ratio was at least 6. In the HBR used in the present study, DS_{BU} and DS_{RA} were 1.44 and 0.032, respectively. The weight-average molecular weight ranged between 10,000 and 30,000 daltons.

HBR Induced No Adverse Effects in Healthy Rats—No adverse reactions were observed during and after intramyocardial injection of HBR in healthy rats. Within 4 weeks, the animals exhibited no cardiovascular complications, such as arrhythmias, pulmonary edema, ascites, or thrombosis. Animal behavior was normal. Histological analysis did not show interstitial edema and inflammatory infiltrates.

HBR Injection into the Infarcted Myocardium Enhanced Myocardial Performance—MRI analysis showed a marked recovery of cardiac performance in infarcted rats treated with HBR, compared with un-treated animals (supplemental Movies 1 and 2). The ejection fraction and cardiac output remarkably recovered in infarcted rats receiving HBR, with significant reduction in LV end diastolic volume 4 weeks after MI (Fig. 1*A*). No major recovery of LV global function was observed 1 or 2 weeks following the injection of HBR (data not shown). LV end systolic wall thickening, an index of regional contractile function, and LV end diastolic thickness, an index of regional mass, were preserved in the LV border zone of infarcted HBR-treated hearts (Fig. 1*B*). Conversely, no increase in contractility and mass was observed in the remote zone (Fig. 1*B*). Cardiac MRI was performed to
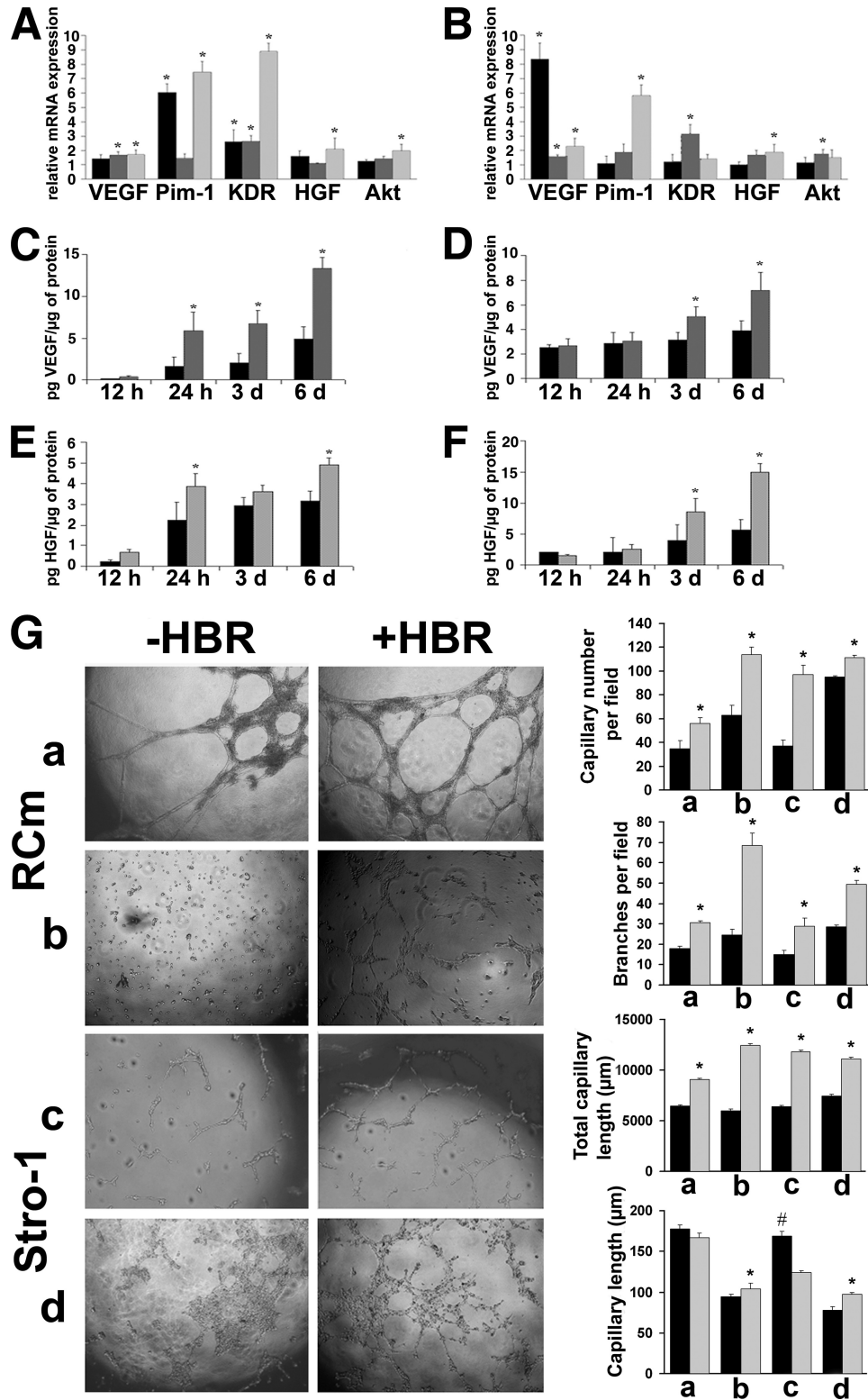
assay kit (B-Bridge International)), according to the user manual. All samples were assayed at least in duplicate.

Western Blotting—Total heart lysate and total lysate of RCm and Stro-1-positive cells were subjected to SDS-PAGE. Acetyl-histone H4 and GAPDH were detected by incubation with a polyclonal rabbit Lys8-acetyl-histone H4-specific antibody (1:1000 dilution; Upstate Biotechnology) and a monoclonal rabbit GAPDH-specific antibody (1:1000 dilution; Cell Signaling), respectively, followed by incubation with horseradish peroxidase-conjugated antibody to rabbit IgG (Cell Signaling). Antigen-antibody complexes were visualized by using ECL

FIGURE 5. **HBR affects gene expression and secretion of trophic mediators.** *A* and *B*, VEGF, *kdr*, HGF, *akt*, and *pim-1* gene expression was assessed by real-time PCR. RCm (*A*) or Stro-1 cells (*B*) were cultured for 24 h (*black bar*), 3 days (*dark gray bar*), and 6 days (*light gray bar*) in the absence or presence of HBR (2 mg/ml). The abundance of each mRNA in untreated cells was defined as 1, and the amounts of VEGF, *kdr*, HGF, *akt*, and *pim-1* mRNA from HBR-treated cells were plotted relative to that value (mean ± S.E.; *n* = 6). *C–F*, time course analysis of VEGF and HGF, respectively, released by RCm (*C* and *E*) or Stro-1 cells (*D* and *F*) cultured in the absence (*black bar*) or presence (*gray bar*) of HBR (mean ± S.E.; *n* = 6). *, significantly different from untreated cells (controls), *p* < 0.05 (GraphPad Prism version 4 (available on the World Wide Web), two-tailed, unpaired Student's *t* test). *G*, *in vitro* capillarogenesis was assessed in HUVECs (*a* and *c*) and RAOECs (*b* and *d*) exposed to a conditioned medium obtained from RCm or Stro-1 cells cultured for 24 h in the absence (*black bar*) or presence (*gray bar*) of HBR. Morphological characteristics of capillary-like networks were evaluated by using NIS-Elements D Nikon software (version 3.06). Data are the mean ± S.E.; *n* = 3. *, significantly different from −HBR; #, significantly different from +HBR; *p* < 0.05.
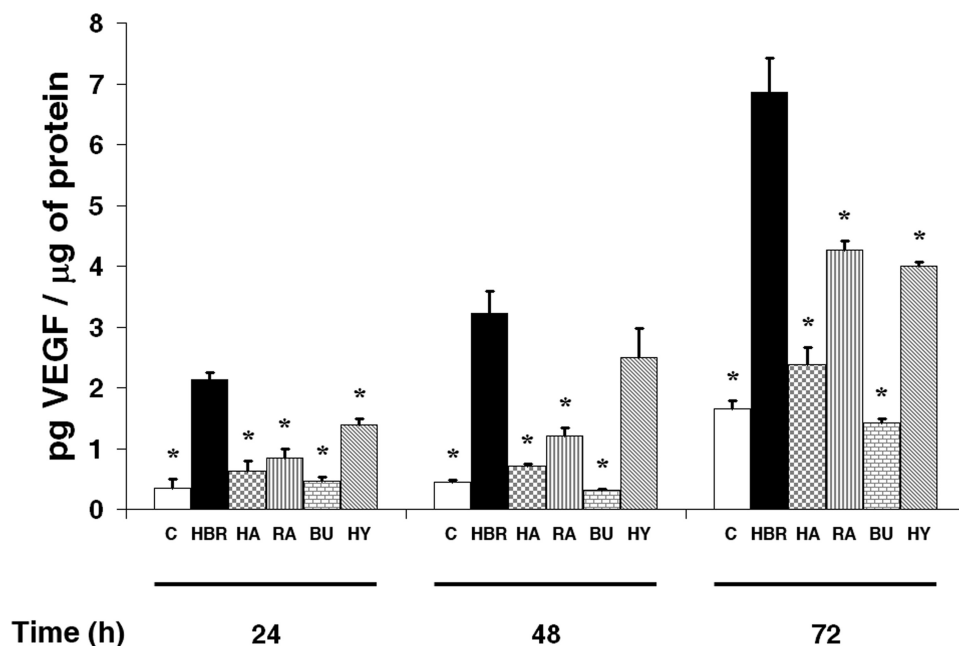
FIGURE 6. Comparative analysis of the effect of HBR, HA, BU, and RA on the secretion of VEGF from rat Stro-1 positive cells. Cells were incubated for the indicated times in the absence or presence of 2.0 mg/ml HBR, 1.5 mg/ml HA, 2.5 mM BU, or 10^{-8} M RA alone or exposed to a hydrolyzed (*HY*) HBR solution (2.0 mg/ml), obtained from a 2-h basic HBR hydrolysis followed by pH neutralization. This procedure has been shown to afford a complete release of each single HBR grafted moiety (C. Ventura *et al.*, unpublished observations). Data are the mean ± S.E. of four separate experiments. *, significantly different from HBR alone (GraphPad Prism version 4 (available on the World Wide Web), two-tailed, unpaired Student's *t* test).

detect scar tissue, which appears hyperintense, and for infarct size assessment in LV injected with PBS or HBR (Fig. 2, *top*). It is noteworthy that we found a significant reduction in the extension of the delayed enhancement of the LV infarct zone in HBR-injected hearts compared with the untreated group (Fig. 2, *top* and *bottom*).

HBR Primed Recovery of Cardiac [^{18}F]FDG Uptake—Fig. 3 displays a polar map of regional distribution and short and long axis images of [^{18}F]FDG uptake in each experimental condition. The ischemic injury in the anterior wall significantly recovered in infarcted hearts receiving HBR (Fig. 3). Glucose metabolism assessed by [^{18}F]FDG uptake, an index of myocardial viability, was also preserved in the border and remote regions of infarcted, HBR-treated hearts (Fig. 3).

HBR Increased Capillary Density and Induced Recruitment of Stro-1-positive Cells—Gross pathologic examination of ischemic myocardium after nitro blue tetrazolium staining revealed that HBR injection substantially decreased the percentage of LV occupied by fibrosis. Picro-Mallory trichrome staining and quantitative analyses showed that the infarct area was significantly smaller in animals receiving HBR than in the untreated group (Fig. 4*A*, *upper images*). Interestingly, in many of the HBR-treated samples, the blue-stained areas, reflecting infarct scarring, were mainly confined to a limited area in the subendocardial zone, which also exhibited regions of viable, red-stained tissue. A terminal deoxynucleotidyltransferase-mediated dUTP nick end labeling assay kit demonstrated that HBR-treated hearts exhibited a decreased number of apoptotic cardiomyocytes when compared with untreated hearts (Fig. 4*A*, *lower images*).

Immunohistochemical analysis of vWF expression revealed that the density of capillary vessels was significantly increased at the infarct border zone of animals injected with HBR, as compared with infarcted tissue receiving saline as a placebo (Fig. 4*B*). Unlike control samples, in the HBR-treated tissue sections, the regeneration of vWF-positive vascular structures was associated with the presence of loose connective tissue in which scattered round and spindle elements were seen embedded; in some samples, this "vascular front" extended from the subepicardial ventricular myocardium and spread into adjacent clusters of "viable" cardiomyocytes. Immunohistochemistry revealed an increased number of perivascular Stro-1-positive cells near newly formed capillaries in HBR-treated hearts after 4 weeks, significantly exceeding the few Stro-1-positive cells detected in the non-injected group (Fig. 4*C*). Interestingly, most of the Stro-1-positive cells lacked staining with vWF (data not shown). On the contrary, some Stro-1-positive cells coexpressed cardiac α-sarcomeric actin (data not shown). On the whole, differently from the Stro-1 expressing elements, the number of c-Kit-positive cells did not differ significantly among treated and untreated animals. This discrepancy may suggest that, at 4 weeks, Stro-1-resident perivascular mesenchymal cells but not c-Kit bone marrow-derived mononuclear cells were selectively embedded in the site of tissue repair following HBR injection.

The presence of Ki-67 was used to determine whether there were cycling cells in the myocardium at the time of sacrifice; after 24 h, a significant increase in Ki-67 expression was found in the examined sections from HBR-injected animals, as compared with the untreated group (Fig. 4*D*). In the HBR-treated hearts, the Ki-67 nuclear antigen was markedly expressed by perivascular spindle- and round-shaped stromal cells located between cardiomyocytes. These cells expressed NG2 and PDGF-Rβ (Fig. 4*E*), a set of markers that have been previously shown to represent a phenotype indicator of pericyte/perivascular identity (12). The same cells lacked expression of hematopoietic cell markers (data not shown). Other Ki-67-positive cytotypes included endothelial cells and polymorphonuclear leukocytes. VEGF cytoplasmic expression also significantly increased in the cardiomyocytes following HBR injection (Fig. 4*F*).

HBR Enhanced the Gene Expression and Secretion of Angiogenic, Antiapoptotic, and Antifibrotic Factors in Both Rat Ventricular Cardiomyocytes and Stro-1-positive Stem Cells—The infarcted myocardium has been shown to release a number of factors, including the granulocyte colony-stimulating factor and the granulocyte-macrophage colony-stimulating factor,

involved in bone marrow cell mobilization and homing (13, 14). No significant difference in plasma levels of each factor was observed throughout a 24-h period between rats sub-

FIGURE 7. **Analysis of VEGF and *pim-1* gene transcription in isolated nuclei.** *A* and *B*, nuclei were isolated from rat Stro-1-positive cells cultured for 24 h (VEGF gene transcription) or 6 days (*pim-1* gene transcription) in the absence or presence of 2.0 mg/ml HBR, respectively. From *lanes C–H*, nuclei were isolated from untreated cells and then directly incubated for 12 h without any drug (*C*) or in the presence of 2.0 mg/ml HBR (*D*), 1.5 mg/ml HA (*E*), 2.5 mм BU (*F*), 10^{-8} м RA (*G*), or with a combination of BU and RA (*H*). Autoradiographic exposure was for 2 days on Kodak X-Omat film with an intensifying screen. The *right side* of each panel shows the position of radiolabeled DNA markers, showing that the single protected fragments migrated with a molecular size comparable with that of VEGF (597 bases), *pim-1* (609 bases), or GAPDH (574 bases) mRNA. Due to the similar size of VEGF-, *pim-1*-, and GAPDH-protected fragments, ^{32}P-labeled nuclear RNA was hybridized separately with cRNA probes, and the corresponding hybrids were run onto different gels. Autoradiograms are representative of six separate experiments.

jected to MI in the absence or presence of HBR (data not shown).

Real-time PCR analysis revealed that *in vitro* exposure to HBR of both RCm and rat Stro-1-positive stem cells significantly enhanced the gene expression of VEGF, *kdr* (encoding a major VEGF receptor), HGF, *akt*, and *pim-1* (Fig. 5, *A* and *B*). In RCm, HBR-mediated stimulation of *pim-1* gene expression occurred in a time-dependent, biphasic fashion. Increased *pim-1* mRNA was detected within 24 h after HBR stimulation and then declined toward basal values after 3 days. A second elevation in *pim-1* gene expression was observed after 6 days of RCm exposure to the mixed ester (Fig. 5*A*).

The HBR treatment enhanced the secretion of VEGF and HGF in the culture medium from both RCm and Stro-1 cells. Time course analyses revealed that the stimulatory action progressively increased during the first 24 h, persisting throughout a 6-day period (Fig. 5, *C–F*). HBR did not appreciably affect the secretion of VEGF or HGF from HUVECs or RAOECs; nor did it induce these cells to form capillary-like structures in a semisolid medium *in vitro* (data not shown). However, a remarkable increase in capillarogenesis was observed when either HUVECs or RAOECs were cultured with medium obtained from cardiomyocytes or Stro-1-positive cells exposed to the mixed ester (Fig. 5*G*). The amount of VEGF released by Stro-1 cells was slightly increased by BU but not HA alone, being significantly augmented by 10^{-8} м all-*trans*-RA, and further enhanced following exposure to hydrolyzed HBR, resulting in the release of all moieties grafted within the mixed ester (Fig. 6). Nevertheless, under these experimental conditions, the yield of growth factor secretion was considerably lower than that detected in HBR-exposed cells (Fig. 6). Cumulatively, these findings suggest the activation of prominent paracrine effects by HBR on both cell populations, enhancing the expression of cytokines and genes with a crucial role in cell survival and angiogenesis.

HBR Acted at the Transcriptional Level—To further dissect the cellular response to HBR, nuclear run-off experiments were designed to assess whether HBR may have affected the rate of gene transcription and whether, in the affirmative, it may have acted as a unit or after hydrolysis of hyaluronan grafted moieties. Fig. 7 shows that nuclei isolated from HBR-treated Stro-1-positive cells exhibited a consistent increase in the transcription rate of VEGF and *pim-1* genes, as compared with nuclei isolated from untreated cells. In separate experiments, nuclei were isolated from
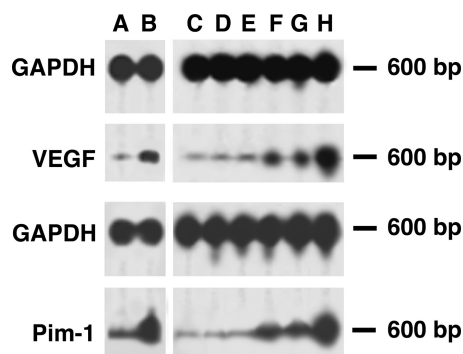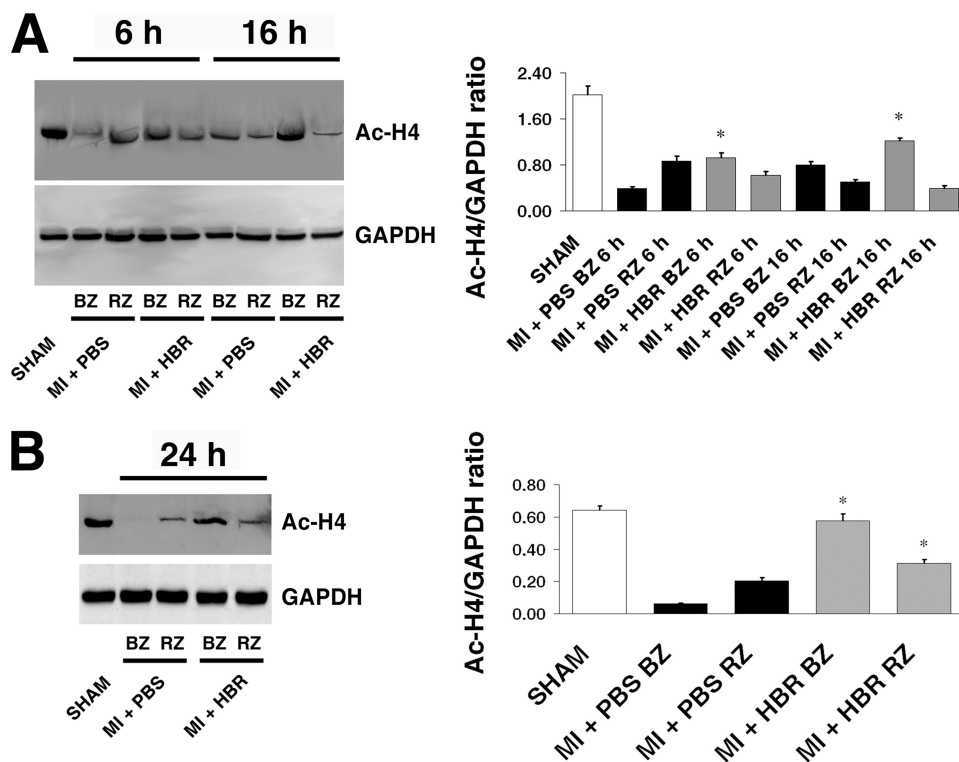

FIGURE 8. **Time course analysis of the effect of HBR on myocardial histone acetylation.** Western blot analysis of histone H4 acetylation was performed in total tissue extracts from border (*BZ*) and remote zone (*RZ*) of infarcted hearts (*MI*) 6 or 16 h (*A*) or 24 h (*B*) after injection in the absence (*PBS*) or presence of 100 μl of HBR solution (0.2 mg of HBR/100 g of rat weight). GAPDH was used as a loading control. Acetylation level was estimated by densitometric quantification (*n = 3*). *, significantly different from the same control time point within the MI BZ (*A*) or from MI BZ or MI RZ (*B*). $p < 0.05$ (GraphPad Prism version 4 (available on the World Wide Web), two-tailed, unpaired Student's *t* test). All Western blots were performed at least three times with similar results.
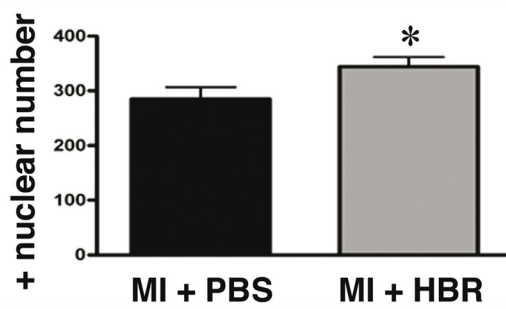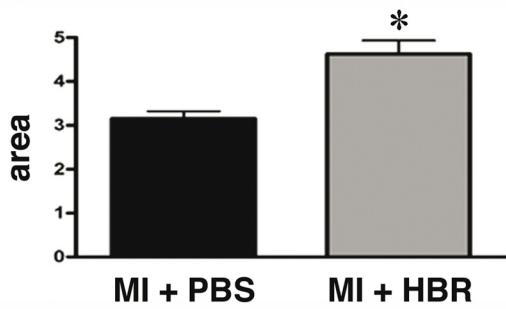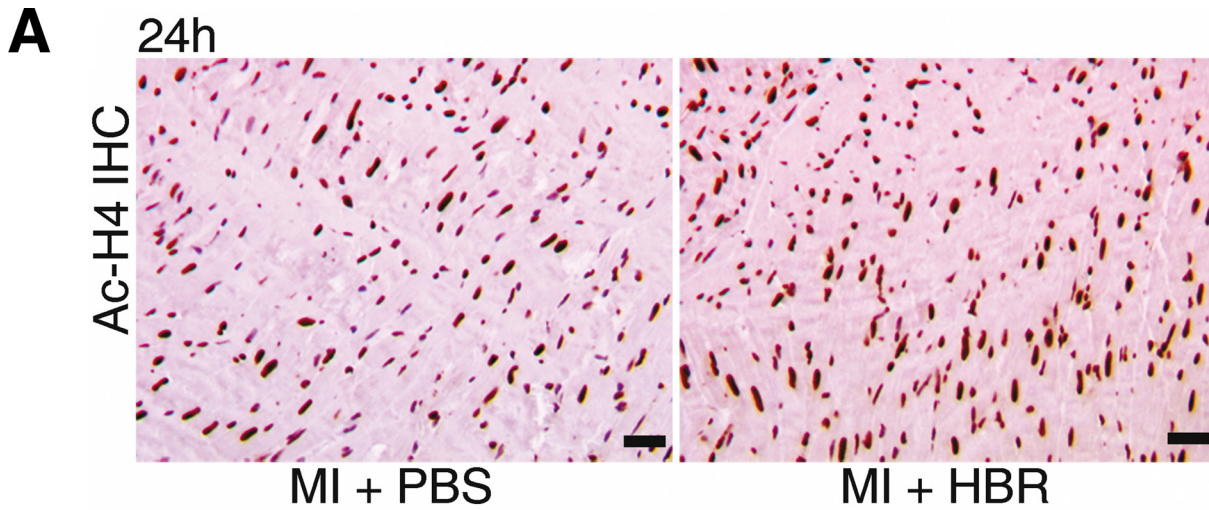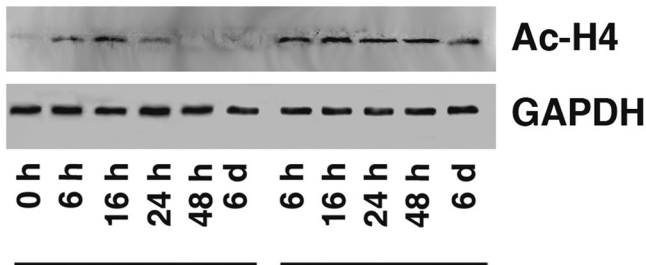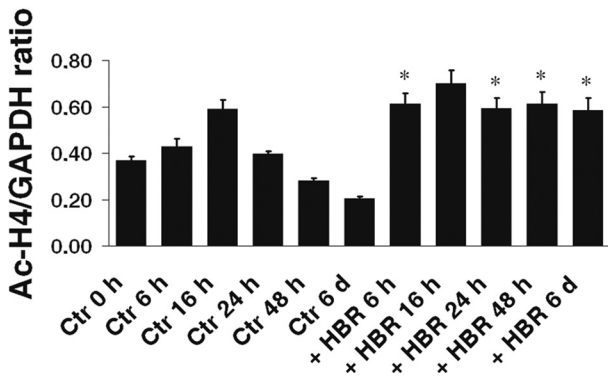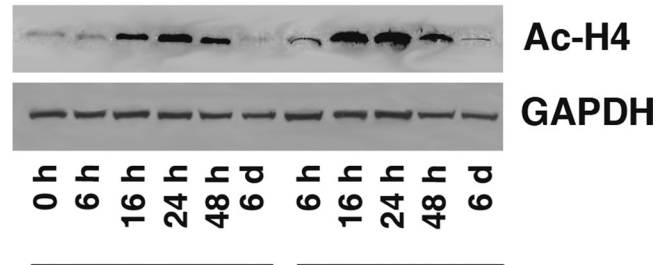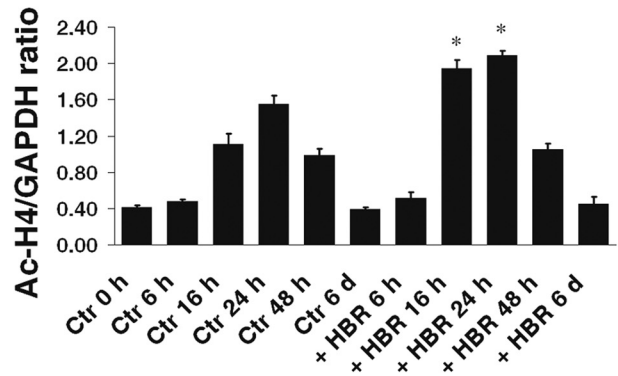
untreated cells and subsequently incubated with HBR or exposed to HA, BU, or RA administered alone or in combination. Although nuclear exposure to HBR or HA failed to trigger a transcriptional response, the incubation with BU or RA enhanced gene transcription (Fig. 7). The transcription rate was further enhanced when nuclei were exposed to a combination of BU and RA (Fig. 7).

HBR Increased Histone Acetylation—Western blot analysis performed in tissue extracts revealed that, consonant with previous observations (15, 16), histone H4 acetylation decreased in the infarcted hearts. Six h after HBR injection, acetyl-histone H4 signal rose in the border zone, progressively increasing up to 16 h, as compared with the untreated group (Fig. 8A). After 24 h, histone H4 acetylation increased both in the border and remote zone of infarcted HBR-injected hearts, as compared with the non-injected tissue (Fig. 8B). Following HBR treatment, a more pronounced signal was detected in the border zone, compared with the remote area. Akin to Western blot studies, immunohistochemical analyses showed an overall increase in the signal of acetyl-histone H4 in hearts of HBR-treated animals, as compared with untreated hearts (Fig. 9A). The number of cardiomyocyte nuclei stained with acetyl-histone H4 antibody was significantly increased by HBR treatment in the border zone (Fig. 9A). *In vitro* experiments provided evidence that acetyl-H4 immunoreactivity was also higher in HBR-exposed RCm and Stro-1-positive cells, as compared with unexposed cells (Fig. 9B).

DISCUSSION

The present study shows for the first time that acute myocardial injection of HBR, a hyaluronan ester previously shown to enhance hMSC-mediated cardiac repair *in vivo* (3), rescued infarcted rat hearts by increasing vascularization, promoting cardiomyocyte survival, and restoring normal tissue function. The HBR action involved an early increase in the number of pericytes, a reserve of progenitor cells that may be integral to the origin of MSCs and other related adult stem cells (12), suggesting a role of perivascular cells in capillary density enhancement and tissue repair elicited by the mixed ester.

It is now evident that an extremely limited percentage of stem cells will engraft and survive within the recipient myocardium following intracoronary infusion or transendocardial injection (17). Moreover, the use of injectable scaffolds to augment stem cell engraftment is not devoid of harmful decrease in myocardial perfusion. Hence, the development of deliverable molecules promoting paracrine mechanisms of cardiac repair and survival of endogenously recruited stem cells, without immediate need of stem cell transplantation, would have remarkable biomedical implications. Here, we show that HBR may fulfill both requirements. Four weeks after HBR injection, a significant increase in perivascular Stro-1-positive cells could be detected within the infarcted hearts. This effect was associated with a reverse myocardial remodeling (decrease of fibrosis and dilatation) and consistent increase in myocardial performance. A possible explanation may result from *in vivo* studies demonstrating that HBR-treated hearts had a significant decrease of apoptotic cardiomyocytes, as revealed by a terminal deoxynucleotidyltransferase-mediated dUTP nick end labeling assay, as well as from *in vitro* experiments showing enhanced gene expression and secretion of VEGF and HGF in both RCm and Stro-1-positive cells exposed to HBR. Growth factor secretion may have primed a proangiogenic context (18), reinforced by the stimulatory effect of HBR on the expression of the *kdr* gene, encoding a VEGF receptor involved in autocrine/paracrine amplification of VEGF secretion and angiogenic signaling (19, 20). Moreover, HGF gene transfer into the myocardium improved myocardial function and geometry (21), due to antifibrotic effects through inhibition of transforming growth factor-β expression. HBR-mediated recruitment of both myocardial and Stro-1 cells into a proangiogenic paracrine circuitry of cardiac repair is further supported by the finding that (i) an increase in capillarogenesis was induced *in vitro* in both HUVECs and RAOECs with a medium obtained from HBR-exposed cells; (ii) no secretion of VEGF or HGF or *in vitro* angiogenesis was found following a direct HUVEC or RAOEC exposure to HBR; and (iii) *in vivo*, a large number of capillary vessels in HBR-injected hearts were "decorated" by Stro-1-positive cells, lacking the expression of vWF, an endothelial marker. Although some Stro-1-positive cells in HBR-injected hearts expressed heart-specific α-sarcomeric actin, these few elements appeared to lack mature sarcomeric organization, and their role in rescuing infarcted myocardium remains questionable.

The observation that exposure of RCm and Stro-1 cells to HBR increased VEGF, HGF, *akt*, and *pim-1* gene expression may have further relevant implications. These genes are deeply involved in cardioprotective signaling, including antiapoptotic and antifibrotic responses (21–25). Enhanced expression of both *akt* and *pim-1* promotes cardiomyocyte survival and growth in transgenic mice subjected to acute myocardial infarction (26, 27). Here, we show that in RCm *pim-1* gene expression was augmented in a biphasic manner by the addition of HBR. Biphasic kinetics in *pim-1* gene expression have been previously demonstrated in other cell types exposed to agents regulating cell growth and differentiation (28, 29) and appeared to involve a complex interplay between cell signaling networks, cell cycle progression, gene transcription, and/or mRNA stability (29). Cardiac control of Pim-1 gene expression is still poorly understood, and future work is required to dissect the molecular mechanisms underlying Pim-1 regulation by HBR in myocardial cells.

HBR may also have increased the survival and rescuing potential of Stro-1-positive cells recruited to the injured myocardium. In this regard, both VEGF and HGF have been shown

FIGURE 9. **HBR increased histone acetylation in infarcted myocardium, isolated cardiomyocytes and Stro-1 cells.** A, immunohistochemistry of acetyl-histone H4. Acetylation level was estimated in infarcted hearts by intensity quantification and counting of stained cardiomyocyte nuclei 24 h after injection in the absence (*PBS*) or presence of HBR solution (0.2 mg of HBR/100 g of rat weight). *Scale bar*, 30 μm. *, significantly different from PBS-treated, $p < 0.05$. B, Western blot analysis of total cell extracts from RCm and Stro-1-positive cells cultured in the absence (*CTR*) or presence of HBR (2 mg/ml) ($n = 3$). *, significantly different from the same control time point, $p < 0.05$ (GraphPad Prism version 4 (available on the World Wide Web), two-tailed, unpaired Student's *t* test). All Western blots were performed at least three times with similar results.

to promote MSC survival and therapeutic potential (30), enhancing stem cell-mediated cardioprotection in infarcted hearts (31, 32). Up-regulation of both *akt* and *pim-1* gene expression in HBR-treated Stro-1 cells is also worthy of consideration, due to the prominent role of these serine/threonine kinases in stem cell survival and differentiation (30, 33). MSCs overexpressing *akt* prevent remodeling and restore performance of infarcted hearts (1, 34). Moreover, *pim-1* has been shown to be required for endothelial and mural cell differentiation *in vitro* (35).

It is relevant that a "program" of genes involved in cardiac protection and stem cell survival can be chemically induced by a synthetic molecule, without the need of viral vector-mediated gene transfer technologies. The molecular dissection of mechanisms underlying HBR-mediated responses *in vitro* and *in vivo* remains to be fully elucidated. The finding that VEGF secretion from these cells was significantly higher in the presence of HBR, as compared with the response to HA, BU, or RA alone, or to a mixture of the three moieties released by hydrolized HBR suggests that a maximal response may be achieved when both BU and RA are concomitantly internalized by the mixed ester. Probably, the exposure to HBR may have afforded an optimal intracellular BU/RA ratio and/or timely action. To this end, nuclear run-off experiments indicate that the action of HBR was mediated at the transcriptional level and that although the transcription rate of VEGF and *pim-1* was unaffected following nuclear exposure to HBR, it was conversely enhanced by BU and RA with superimposable time courses and additive effects. These results also prompt the hypothesis that, at least at the nuclear level, HBR may have acted following the hydrolysis of its grafted moieties.

HBR-induced transcription may be related, at least in part, to the observed increase in histone acetylation, probably attributable to a decrease in HDAC activity by the butyric moiety of the mixed ester. It is evident that chromatin remodeling by HDAC inhibitors can largely affect transcription factor accessibility to target *cis*-acting regulatory sites (36). These so-called epigenetic changes have profound effects on gene expression, both in physiological and pathological processes (36). An inference of the retinoid moiety of HBR with the observed changes in gene expression is supported by the finding that retinoic acid plays a crucial role in mammalian vascular development (37) and enhances angiogenesis by triggering VEGF, *kdr*, and HGF gene transcription and signaling (38). Moreover, retinoid X receptor/retinoic acid receptor heterodimer action is enhanced by histone deacetylase inhibitors, promoting major developmental pathways in pluripotent cells (39). Studies are in progress to further address the spectrum of growth factor and transcriptional profiles recruited by HBR.

The finding that a synthetic glycoconjugate displays a therapeutic effect in the acute phase of MI may have several biomedical implications. In fact, the clinical use of human adult stem cells will be hampered in the near future by a number of inter-related challenges, including (i) high throughput bioprocess development and improved downstream processing problems; (ii) significant modification, improvement, and retesting of current strategies of stem cell culturing and cardiovascular commitment complying with all standards of good manufacturing

practice; and (iii) analytical methodologies for control of good manufacturing practice bioprocessing and differentiation efficiencies. Therefore, the timing for cell culture and expansion within a good manufacturing practice setting will involve a substantial delay (several weeks) in autologous stem cell transplantation with respect to the acute phase of a heart attack. Meanwhile, the cardiac repair afforded by a myocardial injection of HBR may serve as first aid to rescue a damaged heart. This intervention may be followed by delayed transplantation of autologous stem cells, eventually preconditioned *ex vivo* with the same molecule, to enhance the long term potential for cardiovascular cell therapy.

REFERENCES

1. Mangi, A. A., Noiseux, N., Kong, D., He, H., Rezvani, M., Ingwall, J. S., and Dzau, V. J. (2003) *Nat. Med.* **9,** 1195–1201
2. Gnecchi, M., He, H., Noiseux, N., Liang, O. D., Zhang, L., Morello, F., Mu, H., Melo, L. G., Pratt, R. E., Ingwall, J. S., and Dzau, V. J. (2006) *FASEB J.* **20,** 661–669
3. Ventura, C., Cantoni, S., Bianchi, F., Lionetti, V., Cavallini, C., Scarlata, I., Foroni, L., Maioli, M., Bonsi, L., Alviano, F., Fossati, V., Bagnara, G. P., Pasquinelli, G., Recchia, F. A., and Perbellini, A. (2007) *J. Biol. Chem.* **282,** 14243–14252
4. Ventura, C., Maioli, M., Asara, Y., Santoni, D., Scarlata, I., Cantoni, S., and Perbellini, A. (2004) *J. Biol. Chem.* **279,** 23574–23579
5. Fernandes, V. R., Wu, K. C., Rosen, B. D., Schmidt, A., Lardo, A. C., Osman, N., Halperin, H. R., Tomaselli, G., Berger, R., Bluemke, D. A., Marbán, E., and Lima, J. A. (2007) *Radiology* **245,** 712–719
6. Higuchi, T., Nekolla, S. G., Jankaukas, A., Weber, A. W., Huisman, M. C., Reder, S., Ziegler, S. I., Schwaiger, M., and Bengel, F. M. (2007) *J. Nucl. Med.* **48,** 288–294
7. Positano, V., Pingitore, A., Giorgetti, A., Favilli, B., Santarelli, M. F., Landini, L., Marzullo, P., and Lombardi, M. (2005) *J. Cardiovasc. Magn. Reson.* **7,** 487–494
8. Spinelli, A. E., D'Ambrosio, D., Pettinato, C., Trespidi, S., Nanni, C., Ambrosini, V., Baldazzi, G., Bergamini, C., and Marengo, M. (2006) *Nucl. Instrum. Methods Phys. Res. A* **571,** 215–218
9. Bonacchi, M., Nistri, S., Nanni, C., Gelsomino, S., Pini, A., Cinci, L., Maiani, M., Zecchi-Orlandini, S., Lorusso, R., Fanti, S., Silvertown, J., and Bani, D. (2008) *J. Cell Mol. Med.* **13,** 3437–3448
10. Shi, H., Zhang, X., Chen, S., Zhu, W., and Liu, W. (2006) *J. Nucl. Med.* **47,** Suppl. 1, 271P
11. Pfaffl, M. W. (2001) *Nucleic Acids Res.* **29,** e45
12. Crisan, M., Yap, S., Casteilla, L., Chen, C. W., Corselli, M., Park, T. S., Andriolo, G., Sun, B., Zheng, B., Zhang, L., Norotte, C., Teng, P.N., Traas, J., Schugar, R., Deasy, B. M., Badylak, S., Buhring, H. J., Giacobino, J. P., Lazzari, L., Huard, J., and Péault, B. (2008) *Cell Stem Cell* **3,** 301–313
13. Son, B. R., Marquez-Curtis, L. A., Kucia, M., Wysoczynski, M., Turner, A. R., Ratajczak, J., Ratajczak, M. Z., and Janowska-Wieczorek, A. (2006) *Stem Cells* **24,** 1254–1264
14. Napoli, C., Maione, C., Schiano, C., Fiorito, C., and Ignarro, L. J. (2007) *Trends Mol. Med.* **13,** 278–286
15. Lee, T. M., Lin, M. S., and Chang, N. C. (2007) *Am. J. Physiol. Heart Circ. Physiol.* **293,** H968–H977
16. Granger, A., Abdullah, I., Huebner, F., Stout, A., Wang, T., Huebner, T., Epstein, J. A., and Gruber, P. J. (2008) *FASEB J.* **22,** 3549–3560
17. Bonaros, N., Rauf, R., Schachner, T., Laufer, G., and Kocher, A. (2008) *Transplantation* **86,** 1151–1160
18. Tang, Y. L., Zhao, Q., Zhang, Y. C., Cheng, L., Liu, M., Shi, J., Yang, Y. Z., Pan, C., Ge, J., and Phillips, M. I. (2004) *Regul. Pept.* **117,** 3–10

19. Millauer, B., Wizigmann-Voos, S., Schnürch, H., Martinez, R., Møller, N. P. H., Risau, W., and Ullrich, A. (1993) *Cell* **72,** 835– 846

20. Ancelin, M., Chollet-Martin, S., Hervé, M. A., Legrand, C., El Benna, J., and Perrot-Applanat, M. (2004) *Lab. Invest.* **84,** 502–512

21. Li, Y., Takemura, G., Kosai, K., Yuge, K., Nagano, S., Esaki, M., Goto, K., Takahashi, T., Hayakawa, K., Koda, M., Kawase, Y., Maruyama, R., Okada, H., Minatoguchi, S., Mizuguchi, H., Fujiwara, T., and Fujiwara, H. (2003) *Circulation* **107,** 2499 –2506

22. Kaga, S., Zhan, L., Altaf, E., and Maulik, N. (2006) *J. Mol. Cell Cardiol.* **40,** 138 –147

23. Guzman, M. J., Crisostomo, P. R., Wang, M., Markel, T. A., Wang, Y., and Meldrum, D. R. (2008) *J. Surg. Res.* **150,** 286 –292

24. Thirunavukkarasu, M., Addya, S., Juhasz, B., Pant, R., Zhan, L., Surrey, S., Maulik, G., Menon, V. P., and Maulik, N. (2008) *J. Cell Mol. Med.* **12,** 1284 –1302

25. Nakamura, T., Mizuno, S., Matsumoto, K., Sawa, Y., Matsuda, H., and Nakamura, T. (2000) *J. Clin. Invest.* **106,** 1511–1519

26. Matsui, T., Li, L., Wu, J. C., Cook, S. A., Nagoshi, T., Picard, M. H., Liao, R., and Rosenzweig, A. (2002) *J. Biol. Chem.* **277,** 22896 –22901

27. Muraski, J. A., Rota, M., Misao, Y., Fransioli, J., Cottage, C., Gude, N., Esposito, G., Delucchi, F., Arcarese, M., Alvarez, R., Siddiqi, S., Emmanuel, G. N., Wu, W., Fischer, K., Martindale, J. J., Glembotski, C. C., Leri, A., Kajstura, J., Magnuson, N., Berns, A., Beretta, R. M., Houser, S. R., Schaefer, E. M., Anversa, P., and Sussman, M. A. (2007) *Nat. Med.* **13,** 1467–1475

28. Buckley, A. R., Leff, M. A., Buckley, D. J., Magnuson, N. S., de Jong, G., and Gout, P. W. (1996) *Cell Growth Differ.* **7,** 1713–1721

29. Buckley, A. R., and Buckley, D. J. (2000) *Ann. N.Y. Acad. Sci.* **917,** 522–533

30. Rosová, I., Dao, M., Capoccia, B., Link, D., and Nolta, J. A. (2008) *Stem Cells* **26,** 2173–2182

31. Forte, G., Minieri, M., Cossa, P., Antenucci, D., Sala, M., Gnocchi, V., Fiaccavento, R., Carotenuto, F., De Vito, P., Baldini, P. M., Prat, M., and Di Nardo, P. (2006) *Stem Cells* **24,** 23–33

32. Markel, T. A., Wang, Y., Herrmann, J. L., Crisostomo, P. R., Wang, M., Novotny, N. M., Herring, C. M., Tan, J., Lahm, T., and Meldrum, D. R. (2008) *Am. J. Physiol. Heart Circ. Physiol.* **295,** H2308 –H2314

33. Choi, S. C., Kim, S. J., Choi, J. H., Park, C. Y., Shim, W. J., and Lim, D. S. (2008) *Stem Cells Dev.* **17,** 725–736

34. Hammerman, P. S., Fox, C. J., Birnbaum, M. J., and Thompson, C. B. (2005) *Blood* **105,** 4477– 4483

35. Noiseux, N., Gnecchi, M., Lopez-Ilasaca, M., Zhang, L., Solomon, S. D., Deb, A., Dzau, V. J., and Pratt, R. E. (2006) *Mol. Ther.* **14,** 840 – 850

36. Santini, V., Gozzini, A., and Ferrari, G. (2007) *Curr. Drug Metab.* **8,** 383–393

37. Lai, L., Bohnsack, B. L., Niederreither, K., and Hirschi, K. K. (2003) *Development* **130,** 6465– 6474

38. Saito, A., Sugawara, A., Uruno, A., Kudo, M., Kagechika, H., Sato, Y., Owada, Y., Kondo, H., Sato, M., Kurabayashi, M., Imaizumi, M., Tsuchiya, S., and Ito, S. (2007) *Endocrinology* **148,** 1412–1423

39. Dilworth, F. J., Fromental-Ramain, C., Yamamoto, K., and Chambon, P. (2000) *Mol. Cell* **6,** 1049 –1058